An Analytical Formulation to Extract the Capacity Curve of Steel Structures

Abbas Shamivand
Malayer University
Jalal Akbari (j.akbari@basu.ac.ir)
Bu Ali Sina University
Parastoo Allahyari
Islamic Azad University

Research Article

Keywords: Pushover analysis, Nonlinear analysis, Pushover curve, Steel cantilever beam, Large deformations

Posted Date: April 19th, 2022

DOI: https://doi.org/10.21203/rs.3.rs-1540352/v1

An Analytical Formulation to Extract the Capacity Curve of Steel Structures

Abbas Shamivand[1], Jalal Akbari[2*], Parastoo Allahyari[3]

1- Malayer University, Malayer, Iran. ashamivand304@gmail.com, a.shamivand@iaub.ac.ir
2- Associate professor of civil engineering, Laboratory of Health Monitoring of Infrastructures & Energy (LHMIE), Bu Ali Sina University, Hamedan, Iran, j.akbari@basu.ac.ir, akbari@eri.u-tokyo.ac.jp
3- Department of civil engineering, Borujerd Branch, Islamic Azad University, Borujerd, Iran. Parastooallahyari3@gmail.com

Abstract

Among the methods for evaluating the nonlinear performance of structures, pushover analysis is an appropriate alternative instead of direct time history analysis. To accurately extract the capacity curve of a structure, according to the loading regulations/protocols such as FEMA-356 and ATC-40, lateral loads are incrementally applied to the structure in laboratory tests until the structural's failure occurs. Because of the cost and time-consuming nature of experimental tests, proposing mathematical/analytical methods could be the appropriate tools to predict the capacity curves of structures. The present study proposes a new method to find the capacity curves of cantilever steel beams based on mathematical formulations, structural analysis, and material properties. The reason to select a simple beam for this study is to discover all aspects of the system's nonlinear behavior. The strains, stresses, and other responses corresponding to large geometrical deformations have been extracted in two cases with and without strain hardening by considering changes in the behavior of materials. The proposed method has been verified using the finite element method with Abaqus software. The results indicate that the proposed model has acceptable accuracy and could be applied in the pushover analysis of steel structures.

Keywords: Pushover analysis, Nonlinear analysis, Pushover curve, Steel cantilever beam, Large deformations

Nomenclature:

L_u	The length of the beam between the point with M_y and the support	P_U	Collapse load
θ_u	Rotation of L_u	M_U	Collapse moment
θ_{y-B}	The rotation of elastic length of the beam in failure	$M_P = Z * F_y$	Plastic moment
θ_U	Rotation of the whole length of the beam at the point of failure	F_U	The final stress of steel under tension
θ_P	Rotation of L_P	P_P	
θ_{y-P}	Rotation of the elastic length of the beam at the point of plastification of the support	P_y	The load that causes yielding moment at the support
L_P	The length of the beam between the point with M_y and the support for the status of plastification	Δ_u	Displacement of point B due to plastic deformation
δ_y	Displacement of the free end of the beam due to deformation of the elastic length of the beam at the point of plastification of the support	Δ_{y-B}	Displacement of the free end of the beam due to the deformation of the elastic length of the beam at the point of beam failure
Δ_P	Displacement of the free end of the beam caused by P_P	Δ	Displacement of the free end of the beam under P
Δ_y	Displacement of the free end of the beam when the support reaches the yielding moment	δ_P	Displacement of the free end of the beam due to only the plastification of the beam at the support
Δ_H	Horizontal displacement of the free end of the beam	A_g	Area of the beam cross-section
S	Elastic section modulus	$M_y = S * F_y$	Yielding moment
Z	Plastic section modulus	θ	Rotation of the whole beam length
ε_y	Yield strain	d	Beam cross-section depth
ε_U	Strain at the farthest fiber of the section corresponding to the flexural moment of the section failure	ε_P	Strain in the farthest section of fiber corresponding to the plastic flexural moment
μ_θ	The rotational ductility of the beam	$\mu_\emptyset$	Cross-sectional ductility based on curvature (material properties)
E	Modulus of elasticity in the elastic region	μ_Δ	Displacement ductility
ε_{hs}	Strain at the final stress (F_U)	ε_h	Strain at the end of the steel-plastic step

1. Introduction

Researchers in the field of structural and earthquake engineering use pushover analysis, which is a nonlinear static analysis method, to study the behavior of structures, such as large deformations and ductility. Pushover analysis is also applied to investigate the nonlinear performance of structures and is an alternative to time history analysis. To obtain the pushover curve, the structure is constructed in real size or on a smaller scale in the laboratory, and under predetermined instruction according to the loading regulations such as FEMA-356 and ATC-40, the lateral load is applied to the structure so that the structure eventually collapse. Obviously, for steel structures, the first step of the pushover curve is describing their elastic behavior. In the first step, the behavior of the structure is linear and has the highest lateral stiffness, and the deformations are relatively small. When the material experiences inelastic behavior and forming of the first plastic hinge is started, the structure inters into the nonlinear region. Gradually, the lateral stiffness of the structure is reduced until the structure became a mechanism. The last point of this curve indicates the maximum displacement and collapse load of the structure. Also, the area under this curve shows the ductility capacity of the structure.

Push-analysis was applied first in 1975 for systems of one degree of freedom (Freeman, 1975). This method was then gradually developed by other researchers e.g. (Shibaca & Sozen, 1976), (Saiidi & Sozen, 1981), (Fajfar & Fischinger, 1988), (Moghadam, 2002), (Chopra & Goel, 2002).

Currently, the most common method to extract a pushover curve is using experimental methods (Panandikar & Narayan, 2015), (Lian & Su, 2017), (Chen & et al, 2017), (Ferrario & et al, 2016), and numerical methods (Izadinia & et al, 2012), (Peng & et al, 2021), (Shamivand & Akbari, 2020). Some researchers have also used pushover analysis for damage evaluation of structures (Krawinkler & Seneviratna, 1998) (Moghadam & Tso, 2000).

Today, despite many advances in nonlinear inelastic analysis methods, researchers do not use analytical methods to obtain the pushover curve because the structure must tolerate large geometric nonlinear deformations to draw the pushover curve. High accuracy, low cost, and time savings are the advantages of the analytical method in comparison with experimental and numerical methods. Therefore, in this study the authors used concepts such as the first and second moment-area theories, a combination of static equilibrium equations, materials properties, and structural geometry in the case of large deformations, to present an analytical method for extracting the pushover curve for a cantilever beam. The reason to select a simple beam for this study is to discover all aspects of the system's nonlinear behavior. The method presented in this research can obtain the pushover curve point by point and with high accuracy in the inelastic case for nonlinear geometric deformations. Also, by solving the numerical example, it is shown that the strain hardening phenomenon can not be ignored at large deformations, and if the strain hardening phenomenon is ignored, a large error in calculations will occur. In this research, the following assumptions are considered

- The beam has been restrained along the plastic hinge so that damages such as localized web and flange local buckling, diagonal web buckling will not occur
- Lateral buckling will not occur during the beam and the failure of the beam is occurred only due to the rupture of the material.

2. Formulation

2.1. Beam geometry and material properties

According to figure 1, consider the cantilever beam of L length and moment of inertia of I, and the modulus of elasticity of E. To prevent lateral buckling, the beam laterally restraint along its length and is fully fixed in support A, with a concentrated load P applied to its free end.

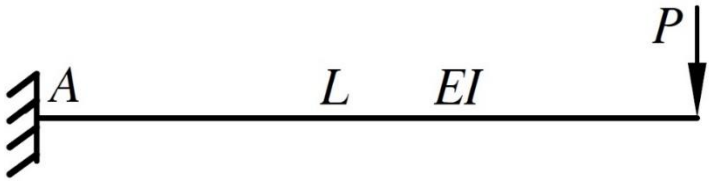

Figure 1: Cantilever beam and loading (top: real beam, bottom: an analytical model of the beam)

If the load uniformly and gradually increases to collapse load (P_U), the free end deflection and the beam length rotation will increase accordingly. During loading, the flexural moment at support A gradually changes from the elastic flexural moment to the flexural yielding moment (M_y) and then to the plastic flexural moment (M_P). If the strain hardening is considered, the flexural moment increases to reach the beam collapse moment (M_U), and if the strain hardening phenomenon is ignored, at the plastic flexural moment, the rotation continues to the collapse point.

In order to correctly apply the material properties, especially the tangential modulus in the inelastic and strain hardening regions of steel, according to figure 2, the modified strain stress curve has been used according to the suggestion of Boeraeve et al. (1993) and Gioncu & Mazzolani, (2003). The stress-strain curve continues until the final steel stress (F_U) with a slope of $E_h = 0.03E$ after reaching the strain ε_h, which corresponds to the end of the steel-plastic step, and after the stress reaches F_U, it continues with a zero slope until it reaches the final strain (ε_U).

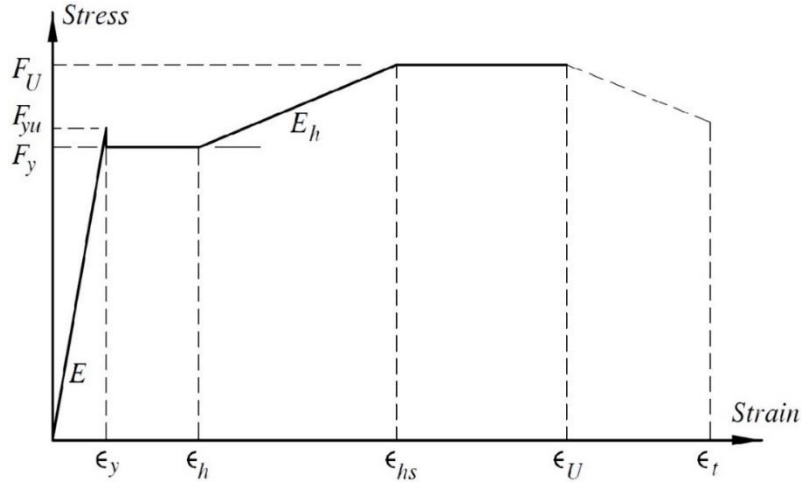

Figure 2: Modified steel strain stress curve in this study

2.2. Small deformations analysis $(P \leq P_y)$

All types of classic analytical methods in structural analysis references, such as virtual work, and first and second moment-area theories could be used to calculate the forces corresponding to elastic small deformation (Kassimali, 2018). At this point, the behavior of the entire length of the beam from the support to the free end is elastic.

2.3. Large deformations analysis $(P > P_y)$

The large deformation involves deformations after the yield point (formation of M_y at the support) which consists of four distinct stages: a- Formation of M_P at the support; b- Reaching the behavior of materials to the end of the steel-plastic step means reaching the maximum strain to ε_h; c -Reaching the maximum stress to F_U or in other words, reaching the maximum strain on the beam cross-section to ε_{hs}; d- Reaching flexural moment at the support to M_U (maximum flexural moment tolerable by the beam section) or in other words, reaching the maximum strain on the beam section to ε_U. If the beam is designed such that local and general buckling failures, crippling under the load, etc. do not occur in the beam and the failure is limited to the failure of the beam caused by the flexural moment reaching the nominal flexural strength of the beam, the curvature diagram ($\emptyset = M/EI$) could be shown in large deformations as shown in Figure 3 (right). The relation of force and moment in elastic rage according to Figure 3 is expressed as equation 1.

$$\boxed{P = \frac{M_A}{L - \Delta_H}} \qquad (1)$$

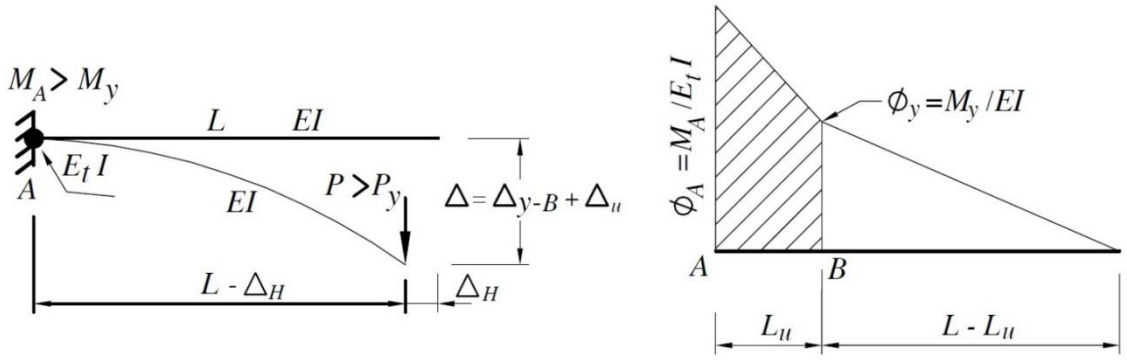

Figure 3: Diagram of curvature along the beam for large deformations (right), beam geometry at large deformations (left)

According to Figure 4, at large deformations, the beam consists of two parts: plastic part (length AB') and elastic part (from point B' to the free end of the beam). In Figure 4a, the parameter θ is the rotation of the whole beam, which consists of two parts: a- the rotation of the beam due to the deformation of the plastic region (θ_u), b- the rotation of the elastic region (θ_{y-U}). In this figure, r is a tangent line at the point B'. Based on the geometry relations, in Figure 4b the arc AB' is approximated by an arc of a circle, the angle of the chord $\overline{AB'}$ along the horizon is equal to $\theta_u/2$ and the length of the chord itself is equal to $\overline{AB'} = (2L_u/\theta_u)sin(\theta_u/2)$. Point B', which corresponds to point B before loading, is the position where the stress is reached to the yielding stress in the farthest section of fiber.

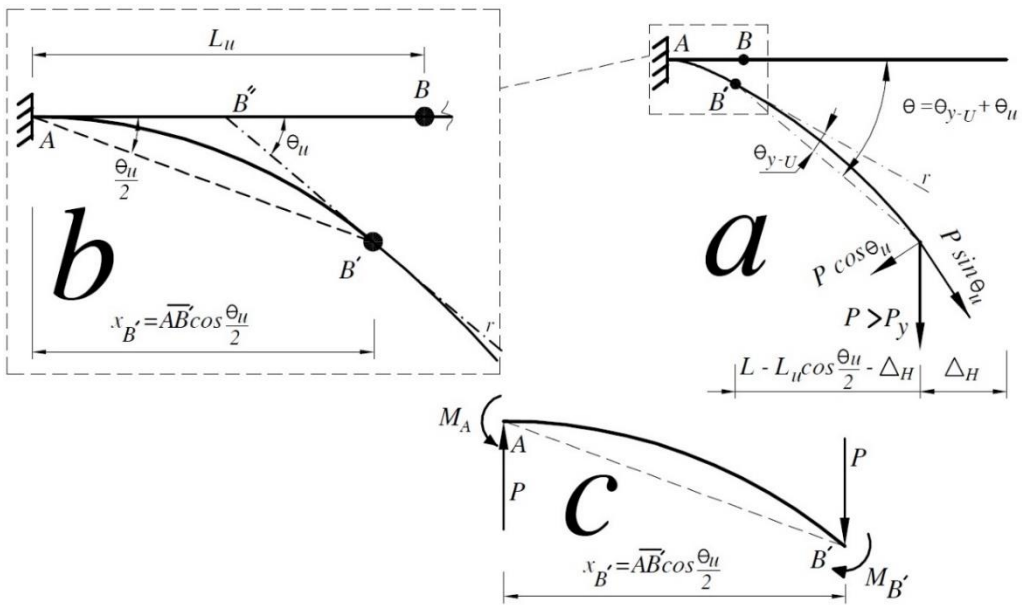

Figure 4: a: Deformed beam geometry at large deformations, b: details of the length A to B, c: Free diagram of AB'

According to Figure 4a, the flexural moment at B' is obtained from equation (2).

$$M_{B'} = P\cos\theta_u * (L - L_u) \qquad (2)$$

Given that the maximum stress in the farthest section of fiber at the point B' (Figure 4a) has reached F_y, based on the superposition principle, equation (3) at point B' is written.

$$\frac{M_{B'}}{S} + \frac{P\sin\theta_u}{A_g} = F_y \quad \rightarrow \quad M_{B'} + \frac{S}{A_g} P\sin\theta_u = M_y \qquad (3)$$

By combining equations (2) and (3) and simplifying them, equation (4) is obtained:

$$L_u\cos\theta_u - \mathrm{L}\cos\theta_u - \frac{S}{A_g}\sin\theta_u + \frac{M_y}{P} = 0 \qquad (4)$$

According to Figure 4c and writing the support-based moment equilibrium equation for part AB', equation (5) is obtained:

$$-M_A + M_{B'} + P.x_{B'} = 0 \qquad (5)$$

By placing the value of $x_{B'}$ in Figure 4b and the value of $M_{B'}$ from equation (2) in Equation (5) and simplifying it, equation (6) is obtained:

$$\left(\frac{\sin\theta_u}{\theta_u} - \cos\theta_u\right) L_u - \frac{M_A}{P} + L\cos\theta_u = 0 \qquad (6)$$

Combining equations (4) and (6), a system of two nonlinear unknown parameters (P and L_u) is obtained according to equation (7).

$$\begin{cases} L_u \cos\theta_u - \mathrm{L}\cos\theta_u - \dfrac{S}{A_g}\sin\theta_u + \dfrac{M_y}{P} = 0 \\ \left(\dfrac{sin\,\theta_u}{\theta_u} - \cos\theta_u\right) L_u - \dfrac{M_A}{P} + L\cos\theta_u = 0 \end{cases} \qquad (7)$$

From the system of equations (7) not only the collapse load (P_U)could be found but also the pushover curve can be obtained in the range of large deformations ($P > P_y$) point by point. By placing $M_y \le M_A \le M_U$, the load P corresponding to M_A can be found. With the values of L_u and P, the value of Δ_H can be obtained from Equation (1). It should be noted that in equation (7) the parameter θ_u is not unknown because according to the first moment-area theory, the area of the hatched area (Figure 3 on the right) is equal to $\tan\theta_u$ and according to the material properties, according to Equation (8) the value θ_u is known in terms of L_u.

$$\tan\theta_u = \left(\emptyset_A + \emptyset_y\right)\frac{L_u}{2} \quad \rightarrow \quad \theta_u = \tan^{-1}\left(\left(\emptyset_A + \emptyset_y\right)\frac{L_u}{2}\right) \qquad (8)$$

Based on the curvature-strain relationship in the section subjected to flexural moment (for small deformations: $\varepsilon = y * \emptyset$ and large deformations: $\varepsilon = y * \tan\emptyset$, y: distance from the neutral fiber), assuming that for the inelastic deformations the relation $\varepsilon = n\varepsilon_y$ is established (for ST37 steel, $\varepsilon_U = 167\varepsilon_y$ means that the value of n at the moment of failure is 167 (Popov, 1990)), it can be concluded that at any curvature such as $\emptyset_A$, the curvature equation can be written in ε_y (Equation (12)). If the strain hardening phenomenon in steel is ignored, $M_U = M_P$, i.e. the cross-section of the beam at a fixed moment $M_P = Z * F_y$ will increase the curvature until it is finally collapsed at the curvature $\emptyset_U$. However, if the strain hardening phenomenon in steel is considered, the flexural moment of the section collapse is equal to $M_U = Z * F_U$ (F_U represents the maximum tolerable tensile stress of steel) which will occur at the curvature $\emptyset_U$ (Figure 5).

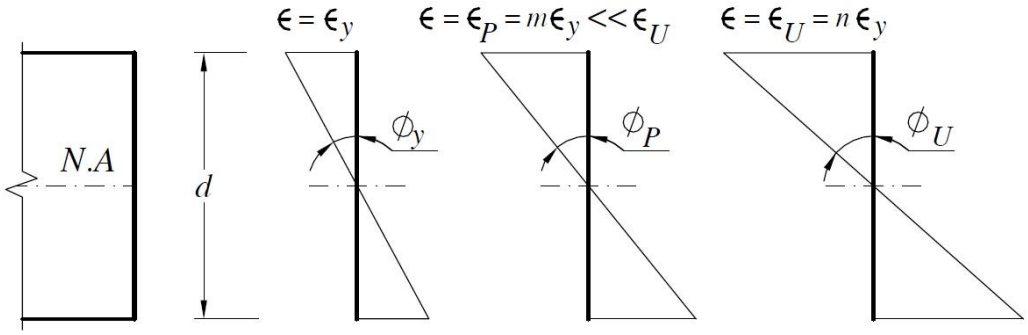

Figure 5: Strain diagram on the cross-section for $\emptyset \ge \emptyset_y$

According to Figure 5 and the assumption that the cross-section of the beam is symmetrical for the flexure axis, the curvature at the moment of failure and the yielding of the section are obtained from Equations (9) and (10), respectively, and by defining, the curvature ductility is equal to the ratio of the collapse ductility to the section yielding ductility (equation 11):

$$\emptyset_U = \tan^{-1}\left(\frac{2\varepsilon_U}{d}\right) \qquad (9)$$

$$\emptyset_y = \frac{M_y}{EI} = \frac{\varepsilon_y}{d/2} = \frac{2\varepsilon_y}{d} \qquad (10)$$

$$\mu_\emptyset = \frac{\emptyset_U}{\emptyset_y} \qquad (11)$$

As well, in the general case of inelastic deformation $(\emptyset_A > \emptyset_y)$, the curvature is obtained according to Equation (12):

$$\emptyset_A = \tan^{-1}(\frac{2 * n\varepsilon_y}{d}) \qquad (12)$$

By substituting $\emptyset_A$ from equation (12) in equation (8), θ_u can be presented in terms of yield strain (ε_y) and L_u in terms of equation (14).

$$\theta_u = \tan^{-1}\left(\left(\tan^{-1}(\frac{2 * n\varepsilon_y}{d}) + \emptyset_y\right)\frac{L_u}{2}\right) \qquad (13)$$

$$\theta_u = \tan^{-1}\left(\left(\tan^{-1}(\frac{2 * n\varepsilon_y}{d}) + \frac{2\varepsilon_y}{d}\right)\frac{L_u}{2}\right) \qquad (14)$$

The free end displacement and the rotation of the elastic part, due to the deformation of the elastic part of the beam, are obtained from equations (15) and (16), respectively.

$$\Delta_{y-B} = \frac{M_y(L - L_u)^2}{3EI} = \frac{F_y S.(L - L_u)^2}{3EI} \qquad (15)$$

$$\theta_{y-B} = \frac{\Delta_{y-B}}{L - L_u} = \frac{F_y S(L - L_u)}{3EI} \qquad (16)$$

When the system of equations (7) for P_U and M_U is solved, the obtained parameter θ_u is correspond to the moment of failure of the beam and can be calculated from equation (17). By definition, rotational ductility is the total rotation at the moment of failure divided by the rotation corresponding to the formation of M_y at the support (equation (18)).

$$\theta_U = \theta_u + \theta_{y-B} \qquad (17)$$

$$\mu_\theta = \frac{\theta_U}{\theta_y} \qquad (18)$$

According to Figures 3 and 4, the total deflection of the free end of the beam consists of three parts: a- Δ_u, which is the deflection of point B, which according to the second moment-area is equal to the moment of the hatched region in Figure 3 around point B, b- deflection due to rotation of the elastic region due to deformation of the plastic region, i.e. $(L - L_u) * \sin\theta_u$, c- Δ_{y-B}, which is the deflection due to deformation of the elastic region $B'C$. The sum of these three parts has been shown in equation (19).

$$\Delta = \Delta_u + (L - L_u)\sin\theta_u + \Delta_{y-B} = \left(\frac{2\emptyset_A + \emptyset_y}{6}\right)L_u^2 + (L - L_u)\sin\theta_u + \Delta_{y-B} \qquad (19)$$

Displacement ductility is the total deflection at the moment of collapse divided by the deflection corresponding to the formation of M_y at the support ($\mu_\Delta = \frac{\Delta_U}{\Delta_y}$).

2.4. Plastic hinge length calculation

The plastic flexural moment (M_P) will occur in the $\emptyset_P$ curvature (Figure 5). Steel sections reach $\emptyset_P$ at the strain much less than ε_h (Figure 2) (this ratio is about 1.1 ~ 1.25 for I-shaped sections), i.e. $\emptyset_P = (1.1\sim1.25)\emptyset_y$ (Chen & Sohal, 2013) and for ST37 steel, $\emptyset_h = 10\emptyset_y$(Popov, 1990). Therefore, in the interval $\emptyset_P$ to $\emptyset_h$, although the strain at the section height will increase significantly, the stress along with the height of the cross-section is constant and equal to F_y. Therefore, at this distance, the flexural moment at a constant cross-section is equal to $M_P = Z * F_y$. If a plastic moment (M_P) is placed in equation (7) instead of M_A (Figure 6), a non-linear equation (20) is obtained instead of a non-linear equation (7):

$$\begin{cases} L_P \cos\theta_P - \mathrm{L}\cos\theta_P - \dfrac{S}{A_g}\sin\theta_P + \dfrac{M_y}{P_P} = 0 \\ \left(\dfrac{sin\,\theta_P}{\theta_P} - \cos\theta_P\right) L_P - \dfrac{M_P}{P_P} + L\cos\theta_P = 0 \end{cases} \quad (20)$$

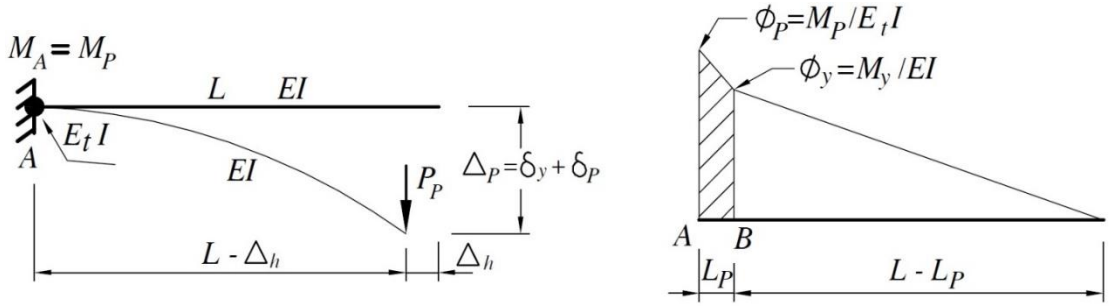

Figure 6: Diagram of curvature (right), loading, and deformed beam geometry (left) when $M_A = M_P$.

By solving the system of nonlinear equations (20), the length L_P and the load P_P and using them the displacement Δ_P, the rotation of the whole beam $(\theta_{y-B} + \theta_P)$, which all correspond to the formation of a plastic hinge at the support A are obtained. Note that due to the strain hardening phenomenon for steel, by forming a plastic hinge at the support, the end of the resistance of the cantilever beam is not reached. As well, by calculating the value of L_u corresponding to M_U by solving the system of equations (7), the length $L_u - L_P$, where the strain of all the fibers at the height of the section has exceeded the yield strain (ε_y), can be calculated.

Considering the very small θ_P, the nonlinear equation system (20) can be replaced by the linear equation system (21) $(\cos\theta_P \cong 1, \sin\theta_P \cong \theta_P)$.

$$\begin{cases} L_P - L - \dfrac{S}{A_g}\theta_P + \dfrac{M_y}{P_P} = 0 \\ -\dfrac{M_P}{P_P} + L = 0 \end{cases} \quad (21)$$

According to Figure 6 (right) if $M_A = M_P$, i.e. for the case where the beam has reached the plastic flexural moment in the support, the area of the hatched region is equal to θ_P, also, by calculating L_P and P_P from the system of equations (21), other parameters such as deflection and rotation can be obtained.

$$\theta_P = (\emptyset_y + \emptyset_P)\frac{L_P}{2} \;\rightarrow\; \theta_P = \frac{(n+1)}{2}\emptyset_y L_P \quad (\emptyset_P = n\,\emptyset_y \;, for\ I\ section\colon\ n = 1.1\sim1.25) \quad (22)$$

3. Results

A cantilever steel (ST37) beam with 3 m length and a given cross-section according to Figure 7 is considered. The pushover curve is plotted for the two modes a and b by the method described in the present study. The stress-strain curve used for steel has been presented in Figure 8. Where F_y is the yielding stress and F_U is the ultimate stress of the steel under tension.

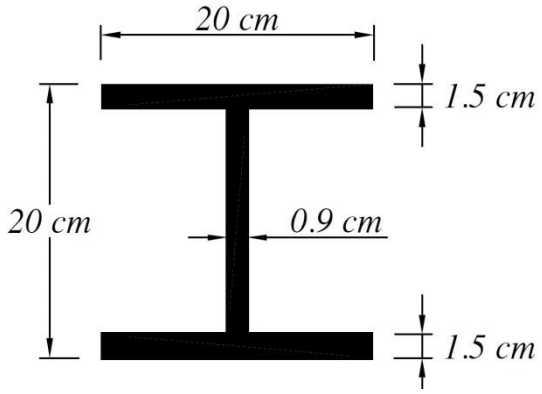

Figure 7: Cross-section of the studied beam

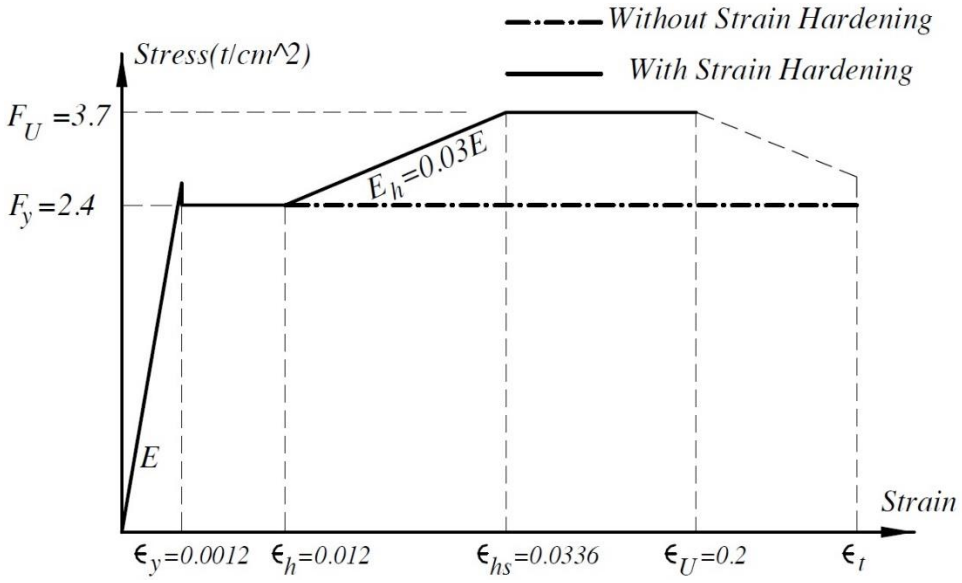

Figure 8: Stress-strain curve (solid line: considering the strain hardening phenomenon dash line: without considering the strain hardening phenomenon)

According to the section geometry, mechanical properties such as the moment of inertia and modulus of elastic and plastic sections are presented in Table 1.

Table 1- Specifications of the beam section

$A_g(m^2)$	$I(m^4)$	$S(m^3)$	$Z(m^3)$	$EI(t.m^2)$
0.00753	$5513 * 10^{-8}$	$551.3 * 10^{-6}$	$619.72 * 10^{-6}$	1108.1

3.1. Small deformations $P = P_y$

If beam analysis is performed for $P = P_y$ with classic analytical methods such as virtual work or the first and second moment-area theories, the results can be calculated in the case of small deformations according to Table 2.

Table 2: Results for small deformations

$A_g(m^2)$	$I(m^4)$	$S(m^3)$	$Z(m^3)$	$EI(t.m^2)$
0.00753	$5513 * 10^{-8}$	$551.3 * 10^{-6}$	$619.72 * 10^{-6}$	1108.1

3.2. Large deformations $P > P_y$

To obtain the coordinates of the points in the pushover curve for $P > P_y$, according to the stress-strain diagram (Figure 8), different points must be investigated and calculated, which are examined below.

3.2.1. Formation of the plastic hinge at the support $(P = P_P)$

According to studies (Chen & Sohal, 2013) for I-shaped sections, there is $\emptyset_P = 1.2\emptyset_y$. According to Table 2 and Figure 5, $\emptyset_P = \frac{2\varepsilon_P}{d} = 0.0144$, thus $\varepsilon_P = 0.00144 < \varepsilon_h = 0.012$, so it can be seen that ε_P is smaller than the strain hardening $(\varepsilon_h = 0.012)$. Therefore, the section of the beam reaches the plastic moment before the strains reach the strain hardness, so the calculations of both modes with and without strain hardening are the same for $M_A = M_P$. Using the system of equations (21), the results are obtained and summarized in Table 3.

$$\begin{cases} L_P - L - \dfrac{S}{A_g} * \theta_P + \dfrac{M_y}{P_P} = 0 \\ -\dfrac{M_P}{P_P} + L = 0 \end{cases} \rightarrow \begin{cases} L_P - 3 - 0.001\, L_P + \dfrac{13.23}{P_P} = 0 \\ P_P = \dfrac{M_P}{L} = \dfrac{14.87}{3} = 4.9567\ ton \end{cases} \rightarrow \ L_P = 0.33\ m$$

$$\boxed{P_P = 4.9567\ ton} \quad , \quad \boxed{L_P = 0.33\ m}$$

Table 3: Results for large deformations ($P = P_P$)

$M_P = Z.F_y$	P_P	$\emptyset_P = 1.2\emptyset_y$	$\delta_y = \dfrac{M_y(L - L_P)^2}{3EI}$	$\delta_P = \left(L - \dfrac{L_P}{2}\right)\sin\theta_P$	$\Delta_P = \delta_y + \delta_P$
$14.87(t.m)$	$4.96(ton)$	$0.0144\left(\dfrac{rad}{m}\right)$	0.028 (m)	$0.0125\ (m)$	$0.0405(m)$

$\theta_P = \dfrac{\emptyset_P + \emptyset_y}{2} * L_P$	$\theta_{y-P} = \dfrac{\delta_y}{L}$	$\theta = \theta_P + \theta_{y-P}$	$L_u = L_P$	$\Delta_H = 3 - \dfrac{M_P}{P_P}$
$0.0132L_P$	$0.0095(rad)$	$0.0139(rad)$	$0.33(m)$	$0.00002 \cong 0$

3.2.2. Results at the end of the plastic step $(P = P_h)$

The end of the plastic step is a fixed point in the steel stress-strain diagram for both cases with and without the strain hardening phenomenon. Therefore, the calculations are the same for both cases. Using the system of equations (7), equation (23) is obtained, that by solving this nonlinear system, the values of L_{uh} and P_h are obtained.

$$\begin{cases} L_{uh}\cos(0.066L_{uh}) - 3\cos(0.066L_{uh}) - 0.073\sin(0.066L_{uh}) + \dfrac{13.23}{P_h} = 0 \\ \left(\dfrac{\sin(0.066L_{uh})}{0.066L_{uh}} - \cos(0.066L_{uh})\right)L_{uh} - \dfrac{14.87}{P_h} + 3\cos(0.066L_{uh}) = 0 \end{cases} \quad (23)$$

Solutions obtained from MATLAB software using fsolve command.

$$\boxed{P_h = 4.9578\ ton} \quad , \quad \boxed{L_{uh} = 0.332\ m}$$

It can be seen that there is no significant difference between P_P (Table 3) and P_h and the reason is that firstly, the distance between ε_P and ε_h in the steel strain stress diagram is very small and second, for both cases, the stress in the total cross-section depth is constant and equal to F_y, so $M_P = M_h$. But the reason for the very small difference between them is that by increasing the free end displacement of the beam from $\Delta_P = 0.0405m$ to $\Delta_h = 0.091m$, the length in flexural moment decreases, and to keep the flexural moment in the support constant, the value of force should be increased from P_P to P_h. Using the results of the system of equations (23), the parameters have been calculated and summarized in Table 4.

Table 4: Results for large deformations ($P = P_h$)

$M_h = z * F_y$	P_h	$\emptyset_h = \frac{\varepsilon_h}{d/2}$	L_{uh}	$\Delta_{uh} = \left(\frac{2\emptyset_h + \emptyset_y}{6}\right) L_{uh}^2$	$\Delta_{y-B} = \frac{M_y (L - L_{uh})^2}{3EI}$
$14.87(t.m)$	$4.96(ton)$	$0.12\left(\frac{rad}{m}\right)$	$0.332(m)$	$0.0046\ (m)$	$0.028\ (m)$

$\Delta_h = \Delta_{uh} + B'C \sin\theta_h + \Delta_{y-B}$	$\theta_{y-B} = \frac{\Delta_{y-B}}{L - L_{uh}}$	$\theta_h = \left(\frac{\emptyset_h + \emptyset_y}{2}\right) L_{uh}$	$\theta = \theta_{y-B} + \theta_h$	$\Delta_H = L - \frac{M_h}{P_h}$
$0.091(m)$	$0.01\ rad$	$0.066 L_{uh}$	$0.032(rad)$	$0.0007(m)$

3.2.3. Results at the end of strain hardening zone ($P = P_{hs}$)

For both cases of with and without strain hardening phenomenon, the strain in the farthest section of the fiber is equal to ε_{hs}, except that in the case of strain hardening phenomenon, the stress in the farthest section of the fiber is F_U, but in the case of ignoring the strain hardening phenomenon, the stress is still constant along with the cross-section and is equal to F_y (Figure 8). The values $\emptyset_{hs}$ and θ_{hs} are obtained from equations (24) and (26).

$$\emptyset_{hs} = \tan^{-1}\left(\frac{\varepsilon_{hs}}{d/_2}\right) = 0.324\ rad/m \qquad (24)$$

$$\tan\theta_{hs} = \frac{\emptyset_{hs} + \emptyset_y}{2} * L_{uhs} = \frac{0.324 + 0.012}{2} * L_{uhs} = 0.168 L_{uhs} \qquad (25)$$

$$\theta_{hs} = \tan^{-1}(0.168 L_{uhs}) \qquad (26)$$

3.2.3.1. Results with considering the strain hardening phenomenon

According to the stress distribution on the cross-section, the flexural moment will be equal to $M_{hs} = 21.27\ t.m$. After substituting the equations (7) in the system of equations and solving it using MATLAB, the following solutions are obtained for L_{uhs} and P_{hs}.

$$\boxed{P_{hs} = 7.186\ ton} \quad , \quad \boxed{L_{uhs} = 1.14\ m}$$

Using the above results, the rest of the necessary parameters such as explained in section 3.2.2 are obtained and presented in Table 5.

Table 5: Results for $P = P_{hs}$ considering strain hardening

$M_{hs}(t.m)$	$P_{hs}(ton)$	$\emptyset_{hs}(rad/m)$	$\Delta_{hs}(m)$	$\theta(rad)$	$L_{uhs}(m)$	$\Delta_H(m)$
21.27	7.186	0.324	0.507	0.1966	1.14	0.04

3.2.3.2. Results without considering the strain hardening phenomenon

In the case of ignoring the strain hardening phenomenon, when the maximum strain on the cross-section reaches ε_{hs}, the stress is still constant at the cross-section depth and equal to F_y (Figure 8), so $M_{hs} = 14.87\ t.m$. After substituting the parameters in the system of equations (7) and solving the device using MATLAB using the fsolve command, the following solutions are obtained for L_{uhs} and P_{hs}.

$$\boxed{P_{hs} = 4.98\ ton} \quad , \quad \boxed{L_{uhs} = 0.337\ m}$$

Using the above results, the rest of the necessary parameters such as section 3.2.2. are obtained, presented in Table 6.

Table 6: Results for $P = P_{hs}$, ignoring strain hardening

$M_{hs}(t.m)$	$P_{hs}(ton)$	$\emptyset_{hs}(rad/m)$	$\Delta_{hs}(m)$	$\theta(rad)$	$L_{uhs}(m)$	$\Delta_{H}(m)$
14.87	4.98	0.324	0.3	0.1052	0.337	**0.014**

3.2.4. Results at the end point of the pushover curve ($P = P_U$)

At the endpoint, due to the maximum strain on the cross-section reaching the strain in which the necking phenomenon occurs in steel, the rupture will occur immediately and it is the end of strength and the beam is collapsed. For both cases of with and without strain hardening phenomenon, the strain in the farthest sectional fiber is equal to ε_U, except that in the case of the strain hardening phenomenon, the stress in the total cross-section depth is constant and equal to F_U, but in the case of ignoring the strain hardening phenomenon, it is equal to F_y (Figure 8). The values of $\emptyset_U$ and θ_u are obtained from equations (27) and (28).

$$\emptyset_U = \tan^{-1}\left(\frac{\varepsilon_U}{d/_2}\right) = \tan^{-1}(2) = 1.107\ rad/m \qquad (27)$$

$$\tan\theta_u = \frac{\emptyset_U + \emptyset_y}{2} * L_u = 0.56L_u \quad \rightarrow \quad \theta_u = \tan^{-1}(0.56L_u) \qquad (28)$$

3.2.4.1. Results considering the strain hardening phenomenon

Considering the constant stress on the cross-section, the flexural moment will be equal to $M_{hs} = z * F_U = 22.93t.m$. After substituting in the system of equations (7) and solving the device using MATLAB, the following solutions are obtained for L_u and P_U.

$$\boxed{P_U = 8.76\ ton} \quad , \quad \boxed{L_u = 1.22\ m}$$

Using the above results, the rest of the necessary parameters such as section 3.2.2 are obtained, presented in Table 7.

Table 7: Results of beam analysis for $P = P_U$ considering strain hardening

$M_U(t.m)$	$P_U(ton)$	$\emptyset_U(rad/m)$	$\Delta_U(m)$	$\theta_U(rad)$	$L_u(m)$	$\Delta_{H}(m)$
22.93	8.76	1.107	1.568	0.6071	1.22	**0.38**

3.2.4.2 Results without considering the strain hardening phenomenon

In the case of ignoring the strain hardening phenomenon, as in sub-section 3.2.3.2, the stress is still constant at the cross-section depth and is equal to F_y (Figure 8), so $M_U = z * F_y = 14.87\ t.m$. After substituting the parameters in the system of equations (7) and solving the system using MATLAB, the following answers are obtained for L_u and P_U.

$$\boxed{P_U = 5.04\ ton} \quad , \quad \boxed{L_u = 0.34\ m}$$

Using the above results, the rest of the necessary parameters such as sub-section 3.2.2 are obtained, which are summarized in Table 8.

Table 8: Results of the beam analysis for $P = P_U$ without considering strain hardening

$\boldsymbol{M_U(t.m)}$	$\boldsymbol{P_U(ton)}$	$\boldsymbol{\emptyset_U(rad/m)}$	$\boldsymbol{\Delta_U(m)}$	$\boldsymbol{\theta_U(rad)}$	$\boldsymbol{L_u(m)}$	$\boldsymbol{\Delta_H(m)}$
14.87	5.04	1.107	0.573	0.2	0.34	**0.05**

According to the calculated results, the curvature, rotational and displacement ductility in the case of with and without considering the strain hardening have been calculated and the results have been presented in Table 9.

Table 9: Ductility of the beam with and without strain hardening

	With strain hardening	*Without strain hardening*	Error (%)
$\mu_\emptyset = \emptyset_U/\emptyset_y$	92.25	92.25	0
$\mu_\theta = \theta_U/\theta_y$	50.59	16.67	203.48
$\mu_\Delta = \Delta_U/\Delta_y$	43.56	15.92	173.62

To conveniently compare the responses in different cases, all results obtained in section 3 are summarized in Table 10.

Table 10: Results obtained from the beam analysis in all cases

		$\boldsymbol{M_A(t.m)}$	$\boldsymbol{P(ton)}$	$\boldsymbol{L_u(m)}$	$\boldsymbol{\emptyset(r/m)}$	$\boldsymbol{\theta(rad)}$	$\boldsymbol{\Delta(m)}$	$\boldsymbol{\Delta_H(m)}$
$P = P_y$	*With strain hardening*	13.23	4.41	–	0.012	0.012	0.036	–
	Without strain hardening	13.23	4.41	–	0.012	0.012	0.036	–
$P = P_P$	*With strain hardening*	14.87	4.96	0.33	0.0144	0.0139	0.0405	–
	Without strain hardening	14.87	4.96	0.33	0.0144	0.0139	0.0405	–
$P = P_h$	*With strain hardening*	14.87	4.96	0.332	0.12	0.032	0.091	0.0007
	Without strain hardening	14.87	4.96	0.332	0.12	0.032	0.091	0.0007
$P = P_{hs}$	*With strain hardening*	21.27	7.186	1.14	0.324	0.189	0.507	0.04
	Without strain hardening	14.87	4.98	0.337	0.55	0.105	0.3	0.014
$P = P_U$	*With strain hardening*	22.93	8.76	1.22	1.107	0.607	1.57	0.38
	Without strain hardening	14.87	5.04	0.34	1.107	0.2	0.573	0.05

Based on the obtained results in all cases the push-over carves (P-Delta, M-Teta) are illustrated in Figures 9 and 10 respectively. According to these figures, the analytical results are compared with the numerical responses using the finite element method. The results show that there is a good agreement between the responses of the proposed analytical method and the numerical method

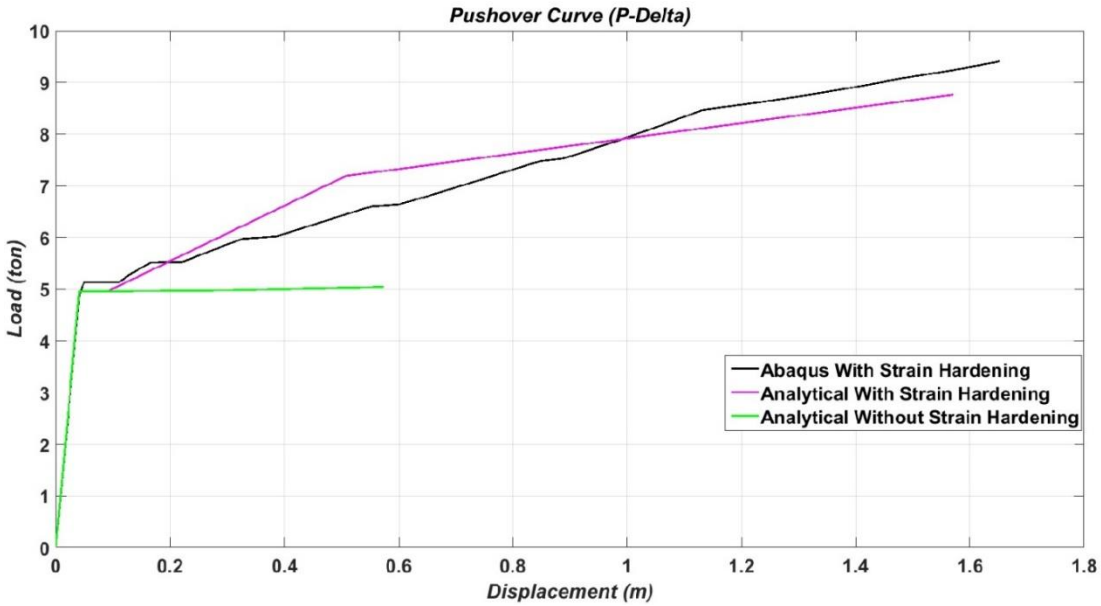

Figure 9: Force-deflection of the free end of the beam (pushover)

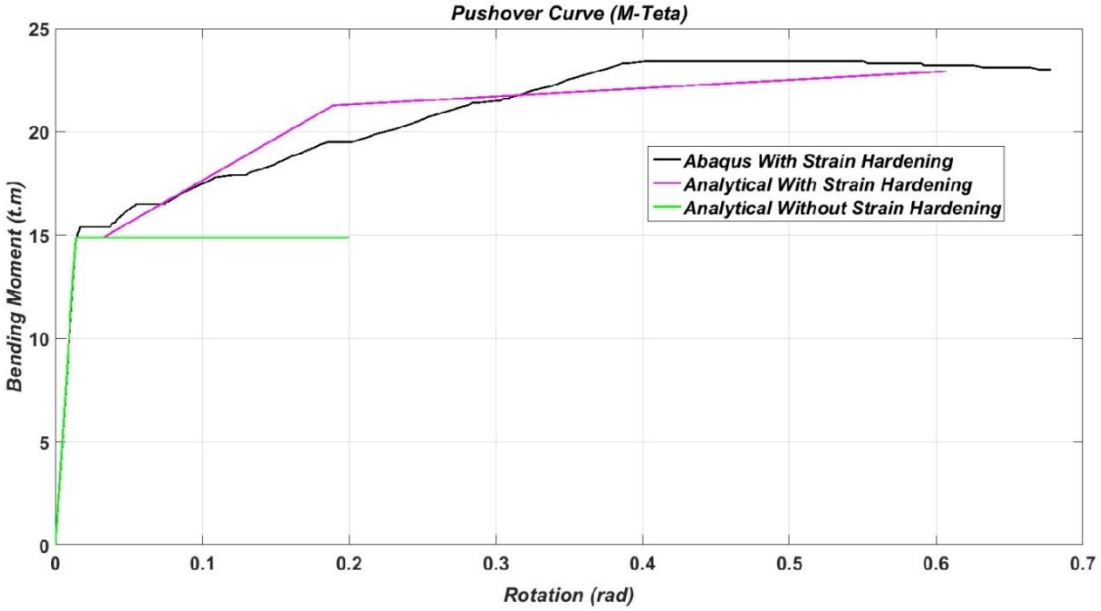

Figure 10: Moment-rotation of the length of the entire beam (pushover)

4. Discussion and conclusion

Based on the studied model, the following results could be drawn.

1- Utilizing the formulations of structural analysis, material properties, and geometry of the deformed structure, the load, and displacement of the structure can be calculated analytically, point by point until the point of collapse and the pushover curve can be obtained for the structure. The advantage of the proposed method is reaching acceptable accuracy instead of using experimental tests or numerical methods.

2- At the deformations corresponding to elastic strain and plastic strain in the range of $\varepsilon \leq 10\varepsilon_y$, the strain hardening phenomenon does not have a significant effect on the behavior of the beam and in nonlinear analysis, its effect can be ignored and the behavior of materials is considered to be elastic perfectly plastic.

3- At large deformations corresponding to $\varepsilon > 10\varepsilon_y$, the effect of the strain hardening phenomenon is significant and it could not be ignored. One of the important effects of strain hardening is that until the moment of collapse, the strength of the material and cross-section is increased and is very significant (Table 9). Therefore, in the case of using the elastic perfectly plastic strain stress diagram, a significant error will be entered into the calculations.

4-According to the results of this study, the plastic flexural moment will increase by about 54% if the effects of strain hardening are taken into account. As well, with the application of the strain hardening phenomenon, the rotational ductility has increased by about 203% and the displacement ductility has increased by about 173%.

5- If the plastic hinge is considered in the region that all of the fibers at the cross-section depth have reached to $(\varepsilon \geq \varepsilon_y)$, the length of the plastic hinge in the case of ignoring the strain hardening phenomenon is zero. Because when the M is equal to M_P in the section, the strain increases in the fibers without increasing the force and without any restriction until the collapse strain (for ST37 steel, $\varepsilon_U = 0.2$). However, despite the strain hardening phenomenon, reaching M to M_P is not the end of the strength and with increasing force, the flexural moment can increase up to M_U. This causes the creation of a space between the M_P location and the M_U the location along with the member. This distance is the length at which the strain of all the fibers at the cross-section depth is greater than ε_y, and in this study, it was found that this distance has a significant value, and in seismic behavior, this length of member plays a main role in the energy dissipation, and increasing the ductility of the system.

Acknowledgment

The second author acknowledged the support of Malayer University when he was an assistant professor of civil engineering from September 2008 to June 2019.

Conflict of interests

The authors have no conflict of interest to declare.

References

Chen, W. F., & Sohal, I. (2013). *Plastic design and second-order analysis of steel frames*. Springer.

Chen, Z., Liu, J., & Yu, Y. (2017). Experimental study on interior connections in modular steel buildings. *Engineering Structures*, *147*, 625-638.

Chopra, A. K., & Goel, R. K. (2002). A modal pushover analysis procedure for estimating seismic demands for buildings. *Earthquake engineering & structural dynamics*, *31*(3), 561-582.

Fajfar, P., & Fischinger, M. (1988, August). N2-A method for non-linear seismic analysis of regular buildings. In *Proceedings of the ninth world conference in earthquake engineering* (Vol. 5, pp. 111-116).

Ferrario, F., Iori, F., Pucinotti, R., & Zandonini, R. (2016). Seismic performance assessment of concentrically braced steel frame buildings with high-strength tubular steel columns. *Journal of Constructional Steel Research*, *121*, 427-440.

Freeman, S. A. (1975). Evaluations of existing buildings for seismic risk-A case study of Puget Sound Naval Shipyard. In *Proc. 1st US Nat. Conf. on Earthquake Engrg., Bremerton, Washington, 1975* (pp. 113-122).

Gioncu, V., & Mazzolani, F. (2003). *Ductility of seismic-resistant steel structures*. CRC Press.

Izadinia, M., Rahgozar, M. A., & Mohammadrezaei, O. (2012). Response modification factor for steel moment-resisting frames by different pushover analysis methods. *Journal of Constructional Steel Research*, *79*, 83-90.

Kassimali, A. (2018). *Structural analysis*. Cengage Learning.

Krawinkler, H., & Seneviratna, G. D. P. K. (1998). Pros and cons of a pushover analysis of seismic performance evaluation. *Engineering structures*, *20*(4-6), 452-464.

Lian, M., & Su, M. (2017). Seismic performance of high-strength steel fabricated eccentrically braced frame with a vertical shear link. *Journal of Constructional Steel Research*, *137*, 262-285.

Moghadam, A. S. (2002). A pushover procedure for tall buildings, proc. In *12th European Conference on Earthquake*.

Moghadam, A. S., & Tso, W. K. (2000). 3-D pushover analysis for damage assessment of buildings.

Peng, J., Hou, C., & Shen, L. (2021). Lateral resistance of multi-story modular buildings using tenon-connected inter-module connections. *Journal of Constructional Steel Research*, *177*, 106453.

Popov, E. P. (1990). Engineering mechanics of solids.

Saiidi, M., & Sozen, M. A. (1981). Simple nonlinear seismic analysis of R/C structures. *Journal of the Structural Division*, *107*(5), 937-953.

Shamivand, A., & Akbari, J. (2020). Ring-shaped lateral bracing system for steel structures. *International Journal of Steel Structures*, *20*(2), 493-503.

Shibaca, A., & Sozen, J. M. (1976). Substitute Structure Method for Seismic Design in Reinforced Concrete. *Journal of Structural Engineering*, *102*, 1-18.